ARTICLE TEMPLATE

Deformation twinning during high temperature compression tests of the Ni-base superalloy ATI 718Plus®

Christiane Kienl[a], Fernando D. León-Cázares[a] and Catherine M. F. Rae[a]

[a] Department of Materials Science and Metallurgy, University of Cambridge, 27 Charles Babbage Road, Cambridge CB3 0FS, UK

ARTICLE HISTORY
Compiled December 27, 2019

ABSTRACT
This study discusses the deformation mechanisms active during high temperature compression tests of the Ni-base superalloy ATI 718Plus®. Deformation twins were observed in deformed grains across a range of temperatures and strain rates by use of transmission electron microscopes (TEM). Even at strain rates as low as $0.01\,s^{-1}$ and temperatures up to 1025°C the microstructure contained of grains which deformed by deformation twinning. It was concluded that the low stacking fault energy of the alloy, which was measured to be $15mJm^{-2}$ caused the formation of the deformation twins. In addition, several examples of the early stages of twin formation were captured. The twinning partials were in most cases emitted from grain boundaries. In a second instance cross-slip events from a Frank-Read source lead to the formation of partials which formed stacking faults.

KEYWORDS
deformation twinning; superalloy; 718Plus; high temperature compression; stacking fault energy

1. Introduction

The characteristics associated with deformation or mechanical twinning in alloys are a combination of high tensile strength and elevated ductility [1]. In face centered cubic (fcc) materials deformation twinning is frequently observed at low temperatures and/or high strain rates [2–5]. But the propensity for deformation twinning of high temperature alloys under forging conditions (temperatures>800°C and strain rates $\sim 0.1 s^{-1}$), is yet to be characterized.

Ni-base superalloys can consist of up to 14 alloying elements forming ordered $L1_2$ γ' precipitates in a disordered γ matrix. Superalloys are well known for forming microtwins during creep at temperatures between 650 and 750°C [6]. Twins have also been studied during thermomechanical fatigue testing of single-crystals at temperatures up to 1000°C [7,8]. However, only a few cases of deformation twinning during high temperature compression tests have been reported [9,10]. In the Ni-base superalloy UNS10276 twins were found after compression tests at temperatures as high as 950°C and strain rates of $10 s^{-1}$ [9]. The tests at strain rates between 0.01 and $1 s^{-1}$ did not show deformation twinning. Similar observations were made for Alloy 617B.

CONTACT C. Kienl. Email: ck492@alumni.cam.ac.uk

Deformation twins started to form at relatively high strain rates of 10 and $20s^{-1}$ temperatures of 1180°C [10]. As with the study by Pu et al. [9], deformation twinning was not reported at the lower strain rates of 0.01, 0.1 and $1s^{-1}$. In both studies twins were only found at high strain rates, in line with the general knowledge of the formation of deformation twins.

Other alloy systems with an fcc structure show a tendency for deformation twinning at high temperatures and low strain rates. Twinning induced plasticity (TWIP) steels, for example, were deliberately designed to form deformation twins leading to high ultimate tensile strength combined with a high ductility [1]. For this type of material it can be shown that they twin even at low strain rates at high temperatures. A study on a transformation induced plasticity (TRIP)-TWIP steel showed deformation twinning during compression tests at strain rates of $0.01s^{-1}$ up to a temperature of 900°C [11]. While the martensitic transformation was operating at temperatures below 150°C, deformation twins were observed in the temperature range from 150-900°C. Eskandari et al. associated the twin formation with simultaneous carbide precipitation which depletes the matrix of carbon and therefore locally decreases the stacking fault energy [11].

Another fcc alloy system is TiAl. TiAl is also known for twinning at temperatures of 750-800°C [5]. TiAl forms lamellae of fcc grains which can serve as a local stress concentrator. It was recently reported, that based on the constraint of grain boundaries, deformation twins are frequently observed in TiAl [12].

Deformation twinning in fcc materials involves the formation and propagation of the same Shockley partial a/6<$\bar{1}\bar{1}$2>on consecutive {111} planes each leaving behind a stacking fault [13]. A number of models have been proposed and reviewed to explain the nucleation of these partials [1,5,14,15]. Twinning partials are supposed to be formed by cross-slip of dislocations in pile-ups, various dislocation reactions within a pile-up or emitted directly from grain boundaries.

This study presents and discusses deformation twinning in a Ni-base superalloy at high temperatures and low strain rates for the first time. The potential reasons for the formation of deformation twins in ATI 718Plus® will be discussed based on testing parameters and material constants. Particular attention will be given to the nucleation and growth of deformation twins.

2. Materials and methods

The material used for this study is the commercial polycrystalline Ni-base superalloy ATI 718Plus®, hereafter 718Plus. It was developed by ATI Speciality Metals and provided by Rolls-Royce plc. with the composition listed in Table 1. The alloy contains a high Nb content resulting in the formation of both γ', the principal strengthening phase, and η phase which can be precipitated at grain boundaries to control grain growth. Depending on the amount of η the γ' fraction was calculated to vary between 19 and 24 mass% T 650°C [16]. In 718Plus γ' is relatively slow to form and grow resulting in a small γ' size between 25 and 30nm after the respective heat treatment [17].

Compression samples were manufactured from the as-received billet. The test pieces were cylinders with the dimensions of 10x15 mm and axes parallel to the billet axis. High temperature compression tests were performed at the Advanced Forming Research Centre at the University of Strathclyde on a servo-hydraulic machine. To simulate an industrial forging procedure, the test temperatures were close to and above the γ' solvus temperatures of 967°C for 718Plus [18]. The samples analyzed for the

Table 1. Chemical Composition of ATI 718Plus® in wt% [20]

	Ni	Cr	Mo	W	Co	Fe	Nb	Ti	Al	C	P	B
718Plus	bal.	18.0	2.75	1.0	9.0	10.0	5.45	0.7	1.45	0.020	0.014	0.004

present investigation were tested at 850, 950, 975 and 1025°C and water-quenched immediately after the test. The strain rate was held constant at either 0.01 or $1s^{-1}$ to three different strains of 0.4, 0.8 and 1.2. The specimens deformed at 850°C were only compressed to a strain of 1. A detailed description of the testing procedure can be found elsewhere [19].

Electron backscattered diffraction (EBSD) was used to obtain a general overview of the microstructure. Samples were cut parallel to the loading axis and mounted on conducting bakelite. After several grinding and polishing steps the specimens received a surface finish with an oxide polishing suspension (OPS) with colloidal silica. The investigation used a Zeiss Gemini 300 secondary electron microscope (SEM) equipped with a Symmetry EBSD detector from Oxford Instruments. The EBSD scans were taken with an acceleration voltage of 25 keV at a sample tilt of 70^o and a step size of 0.15 µm. HKL Channel 5 software was utilized for post-processing of the images where unindexed pixels were cleaned by using the average value of at least six neighboring pixels.

After testing, the samples were prepared for microstructural characterization in a transmission electron microscope (TEM). The compressed cylinders were cut in slices of ∼180 µm parallel to the loading axis and discs spark-eroded from those. The discs were electro-polished using a solution of 10% perchloric acid in methanol at ∼-5°C.

A JEOL 200CX TEM has been used with an operating voltage of 200kV. Scanning transmission electron microscope (STEM) images and electron dispersive X-ray spectroscopy (EDX) were obtained from an FEI Tecnai Osiris at 200KV. The Burgers vector analysis was performed on bright field images in a two-beam condition. The images were taken on six different zone axis with the deviation parameter s being slightly positive. For weak-beam dark dark field (WBDF) imaging the g(3g) condition was selected with the deviation parameter s_{3g} positive.

3. Results

This study analyzes the deformation mechanism of 718Plus after high temperature compression tests. The microstructure of the as-received billet was characterized by TEM and EBSD (see Figure 1). An average grain size of ∼43 µm was obtained from the initial γ-γ' microstructure.

Approximately 20% of the overall grain boundaries were found to be annealing twin boundaries. After the compression tests, only the samples deformed at 850°C retained the γ' precipitates. In the samples tested at all other temperatures γ' dissolved completely and upon quenching the γ matrix was the only detectable phase [21]. This included the samples deformed at a nominal temperature of 950°C, below the reported γ' solvus temperature of 967°C, due to adiabatic heating effects during compression.

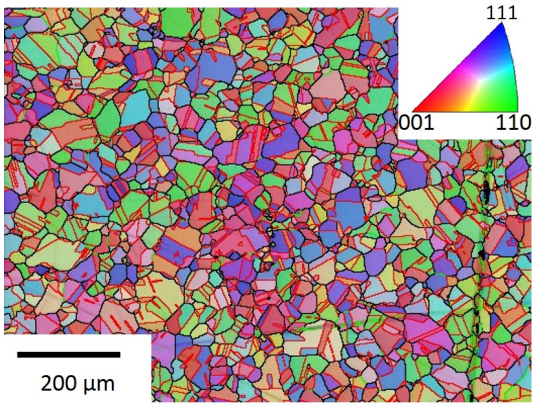

Figure 1. Inverse pole figure map in out-of-plane direction of the as-received billet material 718Plus

3.1. Microstructure of the deformed state

Figure 2a presents flow curves of the cylinders compressed at 850 and 950°C with strain rates of 0.01 and $1\,s^{-1}$. The engineering stress-strain curves were corrected for machine compliance, friction and adiabatic heating. The strengthening effect of the γ' precipitates becomes clear when considering the flow curves. For the γ-γ' microstructure tested at 850°C and a strain rate of $1\,s^{-1}$ the yield point was determined to be 649 MPa. Performing the same test on the γ-matrix at 950°C almost halves the maximum yield stress to 326 MPa.

An inverse pole figure (IPF) map of a specimen compressed with a strain rate of $1\,s^{-1}$ to a strain of 1.2 at 950°C is given in Figure 2b. The map is plotted for orientations normal to the image plane. High angle grain boundaries with a misorientation angle of >15° are drawn in black, low angle grain boundaries are light green and twin boundaries red. The microstructure after testing consists of heavily deformed grains, evidenced by a high orientation gradient within the grains, bordered by much smaller grains with a lower orientation gradient. The latter have recrystallized during the compression test and the microstructure was similar for all conditions tested.

Dynamic recrystallization (DRX) was observed in each sample with varying overall fractions depending on the testing parameters. A typical example of the microstructure after the test is shown in Figure 3a. This TEM bright field (BF) image shows a recrystallized grain (numbered 1 and 2) adjacent to a deformed grain (3). Part 1 of the recrystallized grain includes dislocations as expected for a dynamic recrystallization process. When a new grain forms and continues growing, the dislocation density in this grain will increase due to the ongoing deformation of the sample. Section 1 and 2 are connected via a twin boundary. Annealing twins are commonly observed during the growth of recrystallized grains at the given testing conditions [22] [23]. The contrast of the second part of the grain is homogeneous showing no signs of dislocation activity. Hence, this part must have grown within the 5 s transfer time after the deformation finished and before the sample was quenched. This mechanism is generally referred to meta-dynamic recrystallization. The deformed grain marked with 3 illustrates a high dislocation density with bend contours and fine packets of twins. The respective diffraction pattern (DP) from region 3 is given in the top right corner of the image and shows weak twin diffraction spots. Figure 3b shows a STEM-BF image of part 3 in Figure 3a. The dislocation density and arrangement is due to the work hardening

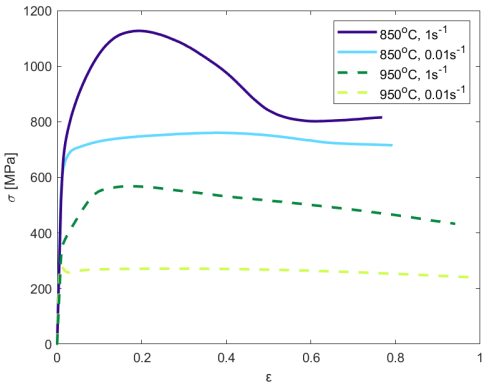

(a)

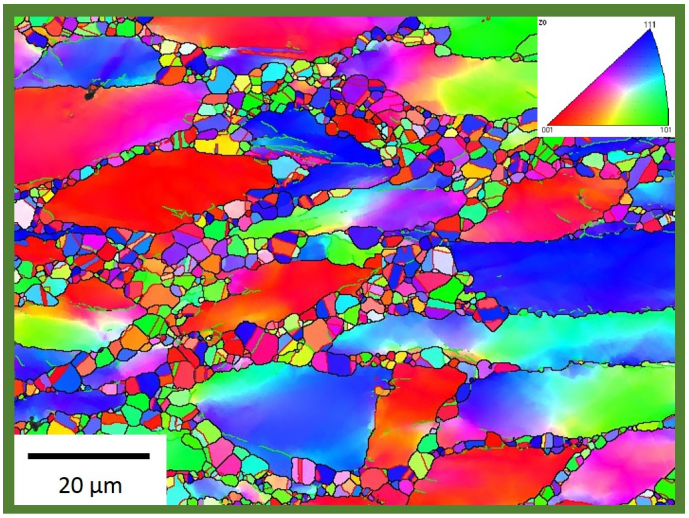

(b)

Figure 2. (Color online) (a) Corrected engineering stress-strain curves of specimens tested at 850 and 950°C (b) IPF map in out-of-plane direction for a sample tested at 950°C to a strain of 1.2 with a strain rate of $1\,\mathrm{s}^{-1}$

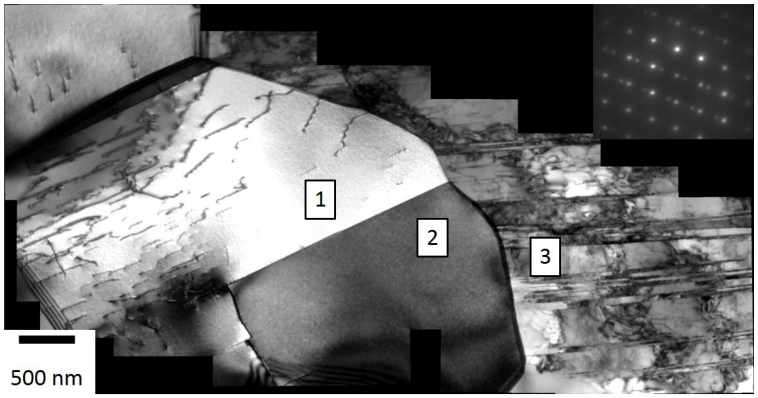

(a)

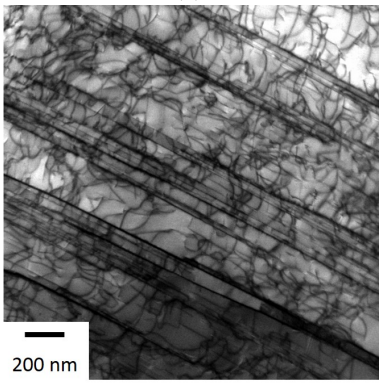

(b)

Figure 3. (a) TEM-BF image of a recrystallized (marked with 1 and 2) and deformed (3) grain with its diffraction pattern in the upper right corner in a sample compressed with a strain rate of $1\,s^{-1}$ to a strain of 1.2 at 975°C (b) STEM-BF image of area 3 in (a)

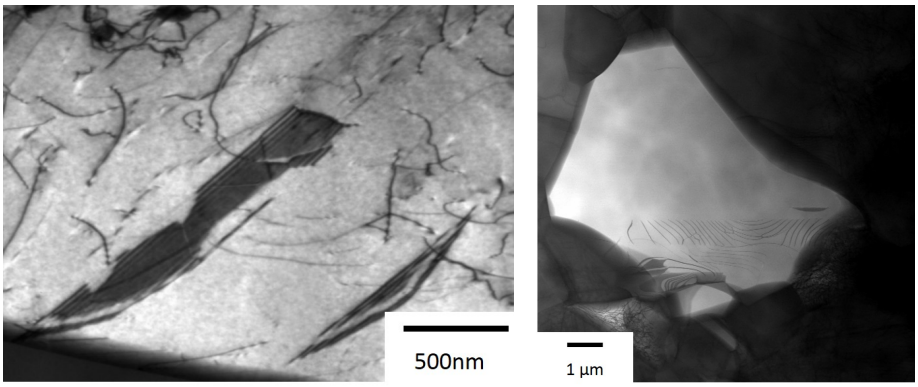

(a) (b)

Figure 4. (a) TEM-BF image of stacking faults in a recrystallized grain (b) STEM-BF image of a dislocation pile-up

taking place during deformation. In addition, the present grain underwent twinning as part of the deformation process.

Further microstructural elements observed were stacking faults (SF) and dislocation pile-ups (Figure 4). Stacking faults are created by a/6<112> partials, the same dislocations are involved in the formation of deformation twins.

The stacking fault energy (SFE) of an alloy determines how far the partial dislocations can separate while gliding through the crystal. The lower the SFE, the larger the separation. As deformation twins consist of overlapping stacking faults, a low SFE is required to initiate twinning and also gives a low coherent twin boundary energy. The stacking fault energy for the γ matrix of nickel-base superalloys are reported to be in the range of 20-30 $\mathrm{mJ\,m^{-2}}$ but can be as low as 11 $\mathrm{mJ\,m^{-2}}$ for the single-crystal experimental alloy UMF and as high as 40 $\mathrm{mJ\,m^{-2}}$ for the polycrystalline U720Li [24–26]. The stacking fault energy of 718Plus has not been reported yet. The observation of stacking fault nodes in Figure 5 provided an opportunity to measure the SFE in 718Plus.

Estimating the SFE can be done by either measuring the distance between two partials or their curvature at a triple junction as imaged in Figure 5s. With the latter method the stacking fault energy γ follows the relationship: [27]

$$\gamma \cong \frac{Gb^2}{4\pi d} \tag{1}$$

with G being the shear modulus, b the Burgers vector and d the equilibrium spacing of the partials. Distance d can further be defined by $R \approx 6d$ with R as the radius marked in the enlargement of Figure 5.

The radii of two triple junctions shown in Figure 5 were selected to calculate the stacking fault energy of 718Plus. The constants in Equation 3.1 were the following: G at 975°C=60 GPa [28] and b=a/6$\langle 112 \rangle$ with the lattice parameter a=3.596Å [29]. Table 2 lists the measured radii and estimated SFE which has an average value of about 15$\mathrm{mJm^{-2}}$.

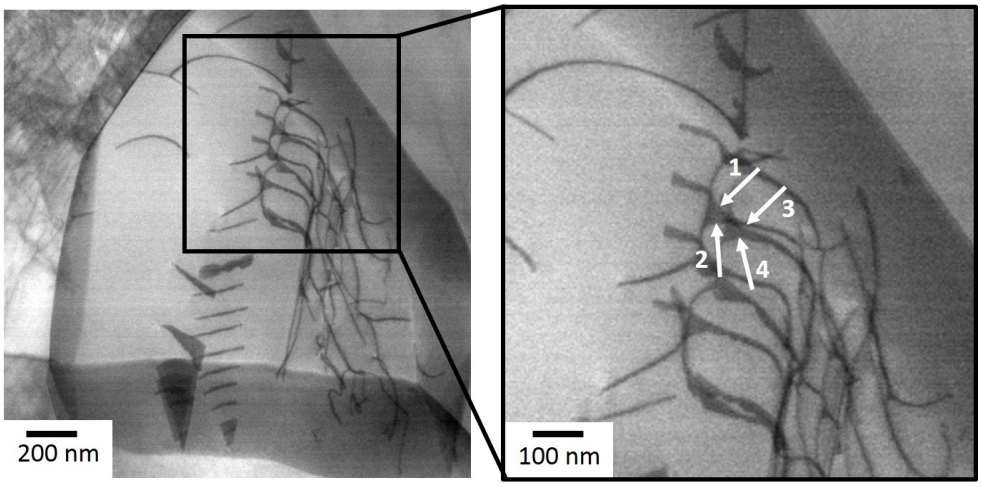

Figure 5. Measured radii at stacking fault nodes in a sample deformed at 975°C.

Table 2. Radii and calculated stacking fault energies for γ in 718Plus

Radius #	R[nm]	γ [mJ m^{-2}]
1	48.5	12.7
2	42.4	14.6
3	36.4	17.0
4	40.4	15.3

3.2. Influence of forging parameters on the deformation mechanisms

High-temperature compression tests were performed above and below the γ' solvus temperature and across a range of strains and strain rates. An in-depth quantification of the deformation mechanisms and the influence of the testing parameters was attempted. Electron channeling contrast imaging (ECCI) on bulk material remained difficult due to the high dislocation density in the grains of interest. TEM foils were therefore the only viable source of information but limited the analyzable area. However, all samples observed at each test condition included at least one grain showing deformation twinning. Deformation twinning in 718Plus during high-temperature compression testing make a significant contribution to strain. An effect of strain and strain rate could not be determined because the limited area observed does not constitute a statistically valid sample.

The samples deformed at the lowest temperature of 850°C showed a notably higher density of deformation twins. As pictured in Figure 6a, the grains in the γ-γ' microstructure have a high dislocation density in addition to the deformation twins. In contrast to the specimens compressed at higher temperatures, the samples from the 850°C tests contain grains with twins on multiple slip systems as illustrated in Figure 6b. The planar twins in the center of the image grew on a different slip system from the narrow twins observable on the right side. The dark patches on top and bottom of the micrograph stem from dense dislocation forests spreading throughout the grain.

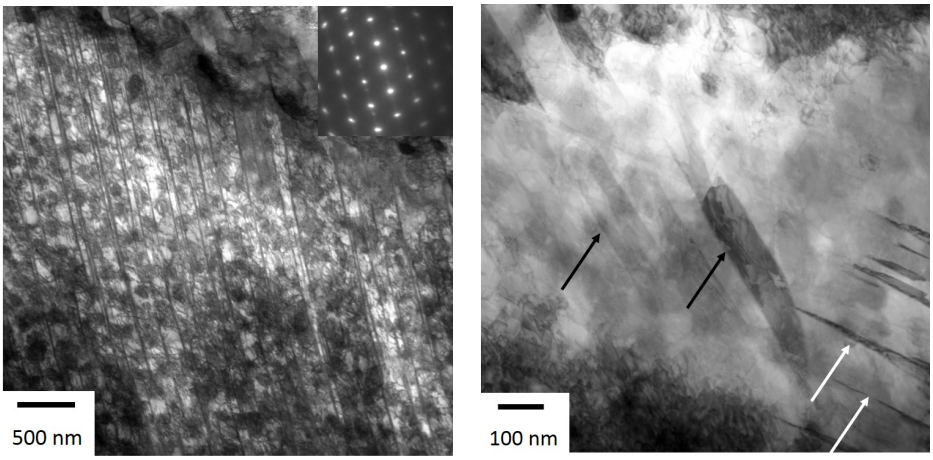

(a) (b)

Figure 6. Samples deformed at 850°C with a strain rate of $1.0\,s^{-1}$ to a strain of 1.0. (a) Twinned grain with a γ-γ' microstructure and the corresponding diffraction pattern (b) Planar (black arrow) and close-to edge-on twins (white arrow) on two different slip systems

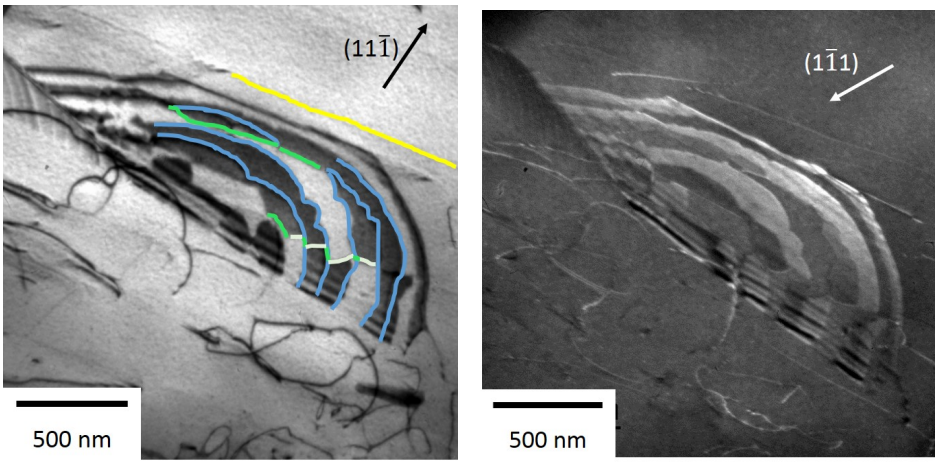

(a) (b)

Figure 7. (Color online) TEM images of partial dislocations from a sample compressed at 975°C to a strain of 1.2 with $1.0\,s^{-1}$. (a) BF on the g-vector of (11$\bar{1}$) with the following dislocation types: yellow: a/2 [101], blue: a/6 [211], white: a/6 [1$\bar{1}$2] and green: a/6 [12$\bar{1}$] (b) WBDF on the g-vector of (1$\bar{1}$1)

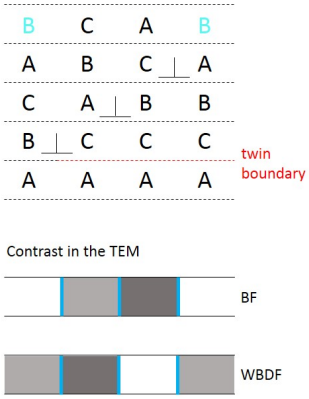

Figure 8. (Color online) Change in contrast with the movement of partial dislocations in an fcc-stacking

3.3. Twin nucleation

Figure 7 shows a series of dislocations in bright-field (BF) and weak beam dark-field (WBDF) conditions for different g-vectors. From the diffraction contrast in Figure 7a-b it can be seen that these defects are partial dislocations leaving behind stacking faults. For a fcc crystal structure with the stacking sequence ABCABC a single partial would change this to ABC*BCA* creating an intrinsic stacking fault (see Figure 8). The change in stacking is seen by the shift in contrast from white to black in the BF-image and from gray to dark-gray in the WBDF condition. If a second partial with the same Burger's vector glides on the {111} plane above, the stacking changes to ABCB*AB* and the contrast BF mode becomes slightly darker and shifts in the WBDF image from dark-gray to white. The third partial on the adjacent plane forms the stacking sequence ABCBA*C* and restores the white contrast in BF and light-gray in WBDF.

The feature described was imaged in six distinct conditions to derive the Burgers vector of the partials. Three different partial types could be identified marked in blue, green and white in Figure 7a. Deformation twins form to compensate the elastic strain field within the grain. As a consequence, the partials within the twin must be largely the same to generate an opposing strain field. This is the case in the example given with the blue partials forming the leading edges of a fan of stacking faults. The active slip plane was determined to be $(1\bar{1}\bar{1})$. The respective partials were of following type: blue: a/6 [211], white: a/6 $[1\bar{1}2]$ and green: a/6 $[12\bar{1}]$. The dislocation highlighted yellow was a matrix dislocation a/2 [101].

The fringes bordering the stacking faults mark the surface of the sample at which the dislocations are cut off. On the left side of the image a wedge-like row of dislocations intersects with the partials.

A similar arrangement of stacking faults was found in an other grain, see Figure 9. The upper part of the bright grain in Figure 9a has a slightly darker area which includes straight as well as more bent dislocations. This area finishes at an almost horizontal border at which the contrast changes to white and dislocations forming fan-shaped overlapping stacking faults. A Burgers vector analysis was performed on this grain with the dislocations identified in Figure 9b. The dislocations were defined for the plane $(\bar{1}1\bar{1})$ and estimated to be: blue: a/6 $[\bar{1}12]$, green: a/6 $[21\bar{1}]$ and yellow: a/2 $[10\bar{1}]$. The yellow full dislocations on the top are arranged in a low angle grain boundary with a strong twist character. The straight nature of the dark purple dislocations appear to be similar to sessile Frank partials defined by Idrissi et al. [30]. However, they do not

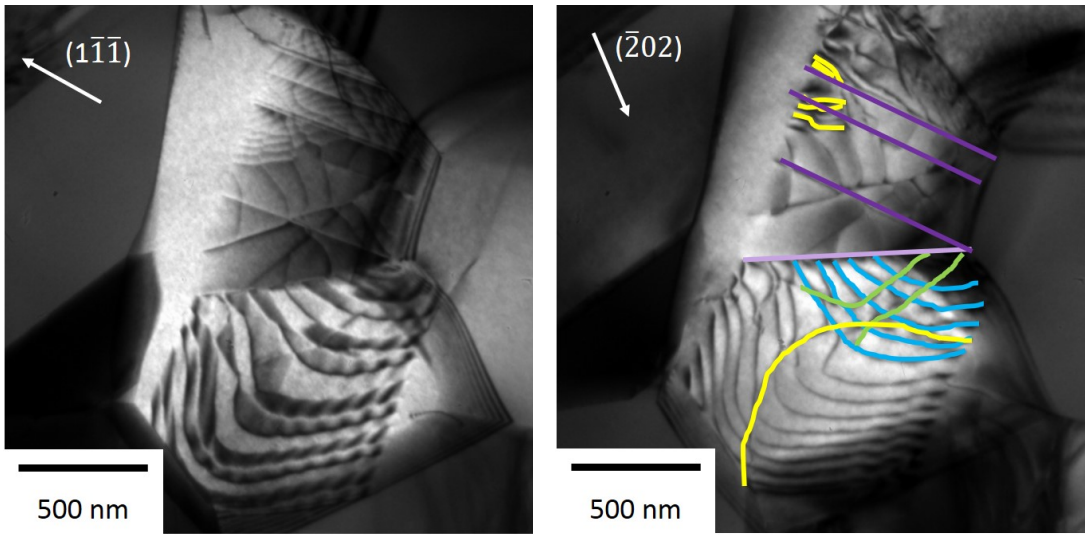

(a) (b)

Figure 9. (Color online) Burger vector study on a sample deformed at 975°C, ϵ=1.2 and $\dot{\epsilon}$=1 s^{-1}. BF on the g-vector of (a) (1$\bar{1}\bar{1}$) and (b) ($\bar{2}$02) and highlighted dislocations with different Burgers vectors: blue: a/6 [$\bar{1}$12] , green: a/6 [21$\bar{1}$] and yellow: a/2 [10$\bar{1}$]

.

seem to disturb the pattern of matrix dislocations. The light purple dislocation marks the border of the low angle grain boundary and the fan of partials at the bottom. Interestingly, the dislocation arrays in the upper part of the image in the low angle grain boundary appear to be fixed. The twin forming partials in the lower section are emerging from a triple point between grains lying within the TEM specimen. This is also the junction where the light purple dislocation and the lowest of the straight, sessile dislocations meet. Thus the twinning partials are generated where a low angle grain boundary in one grain meets the other grains, potentially a point of high stress.

Figure 10a presents the formation of a stacking fault with both partials, the leading and the trailing, visible. The micrograph is colored to identify the dislocations. A Burgers vector analysis of the dislocations revealed the following types for the plane ($\bar{1}1\bar{1}$): turquoise: a/2 $\langle 10\bar{1}\rangle$ (111), brown: a/6 [1$\bar{1}\bar{2}$], beige: a/6 [21$\bar{1}$] and yellow: a/2 [1$\bar{1}$0]($\bar{1}$11). The dislocations form stacking faults as they move into the center of the grain, away from the twin boundaries. In this case, the trailing partial can follow the leading partial and hence does not form a twin. The stacking faults do not overlap because their contrast does not change.

The grain also has two annealing twin boundaries marked with TB1 along the upper part and TB2 at the bottom. To explain the dislocation configuration, a 3D visualization with MATLAB from TEM-images of six different orientations [31]. In the 3D visualization the dislocations are colored according to the slip plane they are operating on. In this case, three different slip systems are active marked in red, blue and green.

The origin of the dislocations active on the blue plane (close to the specimen plane) is a Frank Read source (FR) close to the twin boundary TB1 but separate from it. The segment bowing out on the blue plane is connected to two segments on the red plane pointing up and down through the thickness of the specimen. The dislocations thus generated appear to punch through this twin boundary, into the annealing twin, TB1,

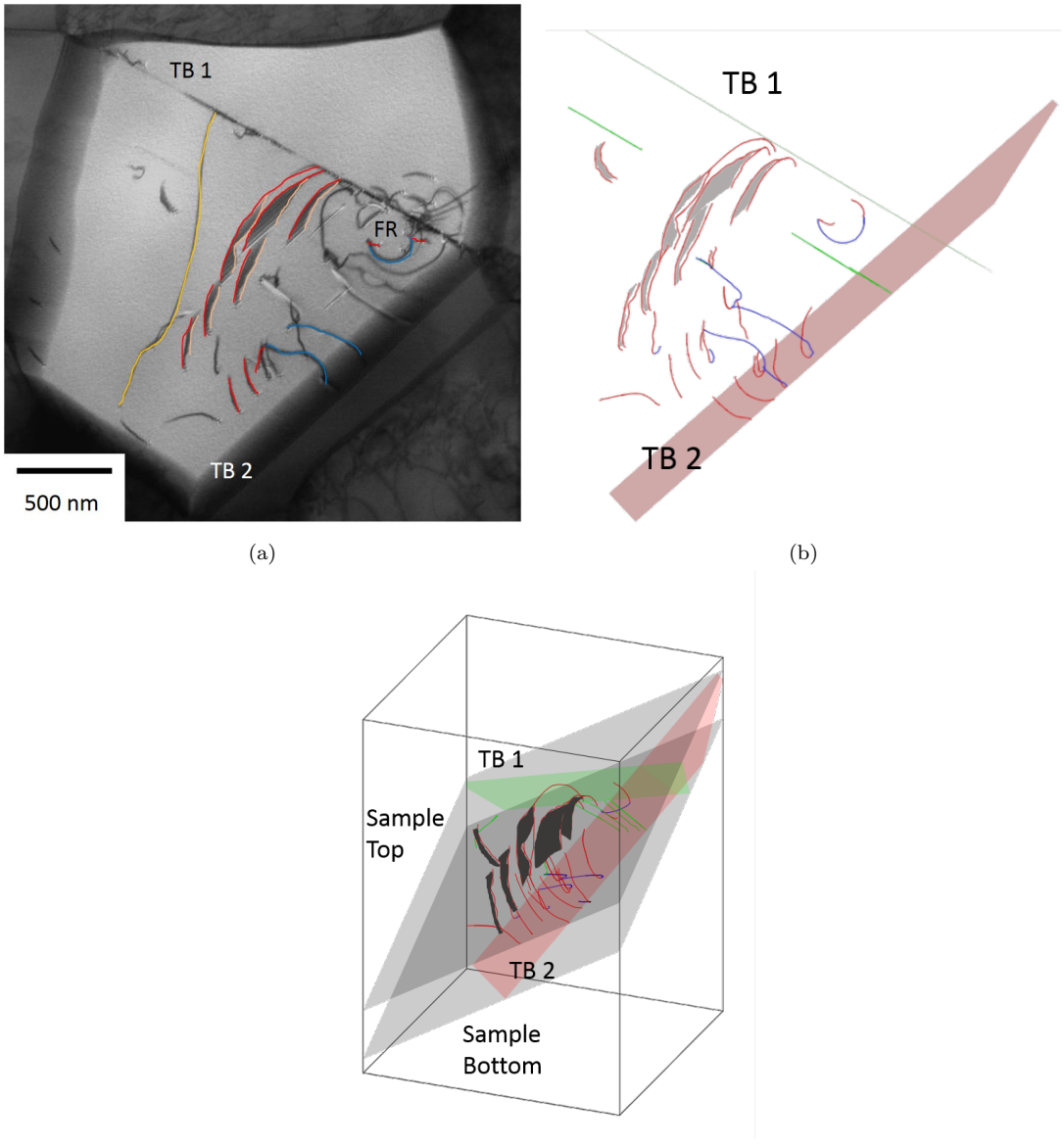

(a) (b)

(c)

Figure 10. (Color online) Sample deformed at 975°C, ϵ=1.2 and $\dot{\epsilon}$=1 s^{-1} (a) STEM image of stacking faults and dislocation activity on multiple slip systems (b) and (c) 3D visualization of (a)

at the top of the figure. There are four separate arrays of red dislocations generated on parallel planes: these too seem likely to be generated from Frank Read sources not captured in the specimen section. However, the cross-slip of the blue dislocation between the blue and red slip planes, creates short sections both suitable to act as dislocation sources.

From the 3D visualization it can be observed, that the splitting of the dislocation into partials only occurs on the red plane and is in excess of around 200μm. It seems that the resolved shear stress on that specific plane favors the separation of partials.

4. Discussion

The present study reveals the deformation mechanisms active in the nickel-base superalloy 718Plus during high temperature compression tests equivalent to conditions typical of forging practice. Formation of stacking faults and deformation twinning make a significant contribution to strain in all samples, together with dislocation pile-ups. Within the grains showing very high dislocation density, packs of 'mature' twins were present, some spanning the whole grain. During the tests, dynamic recrystallization was activated leading to a partially recrystallized microstructure. This resulted in a heterogeneous microstructure where heavily deformed grains could be analyzed alongside newly recrystallized ones. Within the recrystallized grains, dynamic and metadynamic recrystallization could be clearly distinguished. The initial stages of twin formation were captured in recrystallized grains. In the following discussion, the occurrence of deformation twins based on testing and material parameters will be discussed together with the mechanism for the twin formation.

4.1. Parameters for the formation of deformation twins

The experimental parameters for the compression tests covered a wide range of temperatures, strain rates and strains. Within the constraints of the current study, there was no detectable effect of temperature on the propensity for twinning above the γ' solvus between 950 and 1025°C. However, lowering the test temperature to 850°C, being γ' sub-solvus, showed a distinct increase in the degree of twinning within grains and also resulted in twinning on multiple planes. The influence of temperature is complex in nature.

- Firstly, the movement of edge dislocations by climb is vital to recovery processes and is controlled by diffusion. For conventional single phase fcc alloys, raising the temperature increases the diffusion rate. This makes recovery easier and lowers the need for alternative deformation mechanisms such as twinning [5]. In the present study, no link between the rate of recovery and twinning could be observed. TiAl, however shows the opposite trend with an increase in deformation twinning with temperature. This was reasoned to be related to the lamellar nature of the alloy where co-ordinated twinning can reduce the constraint generated at neighboring colonies [12].
- Secondly, the testing temperature determines whether the microstructure is single (γ) or two-phase (γ-γ'). In nickel-base superalloys the γ' precipitates hinder the dislocation movement by glide [32]. In γ-γ' superalloys twinning requires activation to pass through ordered precipitates, and hence tends to be a high-temperature phenomena during creep in several nickel-base alloys [33,34].

Stacking fault energies generated during twinning can be lower than anti-phase boundary (APB) energies in γ' but require thermally activated re-ordering to occur [34]. Although mostly deformed in the supersolvus condition, the 718Plus remains close to the solvus and may experience short range order effects.

- The temperature dependence of the SFE of superalloys is still under debate. Recent theoretical studies claim a decrease of the SFE of nickel with temperature, contradicting the common assumptions based on CALPHAD calculations of the relative Enthalpies of the fcc and hcp phases [35–37]. It was also shown by Shang et al., that the γ' forming elements Al and Ti further decrease the SFE of Ni [36]. Thus above the γ' solvus the effect of temperature on twinning is complex. Overall based on the most recent modeling and the effect of dissolving the γ' one would expect a decrease in SFE with temperature. In this analysis, the SFE of the γ phase was measured to be 15mJm^{-2}. Such a low SFE facilitates the movement of partial dislocations with a large spacing between and hence the frequent nucleation of deformation twins. The SFE of superalloys are reported to range between 20 and 30mJm^{-2} [24]

In terms of the role of temperature on twinning in 718Plus, the mechanism appears to be less affected directly by the appearance of ordered precipitates than by the ability of the dislocations to recover. A decrease in SFE with temperature is competing with the ease of climb rising with temperature. Hence it is perhaps not surprising that the influence of temperature on the amount of twinning is not pronounced.

High strain rates and severe plastic deformation are frequently reported to trigger deformation twinning in Ni-base superalloys [9,10]. Twins have been found after high temperature compression tests for strain rates of 10 and 20 s^{-1}. At high strain rates the dislocations have less time to reduce the overall energy by thermally activated recovery processes. Hence, twinning provides an alternative mechanism which is less inhibited by dislocation density, and indeed may be facilitated by moderate amounts of slip. In the present study twinning was observed at strain rates as low as 0.01 s^{-1}, but was more common at the higher strain rates, albeit relying on observations from a limited number of grains. In TWIP Steels [1], the argument is made that a certain level of strain needs to be achieved to reach the critical resolved shear stress on the twinning plane. This involves dislocation activity leading to work-hardening. It implies that twinning requires more stress than initial dislocation motion. Hence, in TWIP steels twinning is preferred in larger grains (>3 μm [1]) and high strain rates where sufficient work-hardening can be achieved. The observations here do not suggest that twinning requires significantly more stress than dislocation motion, although it is clear that the twinning mechanisms proposed in section 4.3 require dislocation activity in order to operate [38]. Twinning in this study is seen to be operating in newly recrystallized grains with, overall, a very low level of dislocation density. The three strain levels in this study, 0.4, 0.8 and 1.2, had no influence on the amount and appearance of, the twins. Closely packed deformation twins were only observed in grains present before the compression test: within recrystallized grains deformation twins were always in the early stages of formation.

4.2. Chemical effects: segregation and phase formation

In an fcc lattice, twins locally form an hcp structure. Alloy 718Plus precipitates η phase, an hcp-phase with the crystal structure $D0_{24}$. The nose of the TTT-diagram of η was experimentally determined to be at around 950°C [18]. As the compression tests

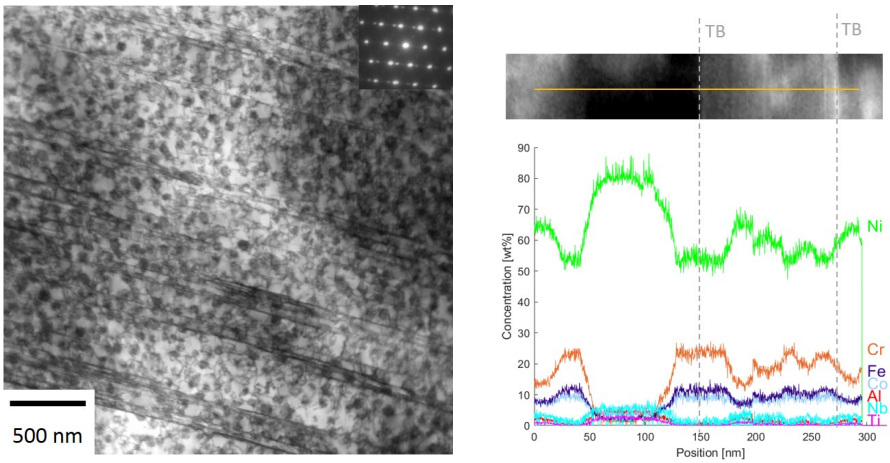

(a) (b)

Figure 11. (Color online) Sample deformed at 850°C with a strain rate of $0.01\,s^{-1}$ to a strain of 1.0. (a) Heavily twinned γ-γ' microstructure (b) EDX-linescan across several twin boundaries (TB).

were performed in this temperature range it is possible that η starts precipitating in the metastable γ matrix preferring a site that is already hexagonal. An alternative, but equivalent, view would be that appropriate elements partitioning to the η phase, (Nb and Ti) would segregate to such a fault effectively lowering the SFE. To check whether this could be a contributory factor in twinning, EDX measurements on twin boundaries were performed on samples deformed at 850°C. Figure 11b presents the results of a linescan across twin boundaries on edge in a sample deformed at 850°C with a strain rate of $0.01\,s^{-1}$ (Figure 11b). The dark area on the left side of the first twin boundary is a γ' particle in diffraction, seen by the increase of Ti, Al and Nb and the decrease in Cr, Co and Fe. Another precipitate is detected at the position 180-200 nm, close to the end of the scan. The scan shows several peaks at and in between the twin boundaries, but they tend to be consistent with either γ or γ' forming elements. The scan crosses twin boundaries in both phases without distinct peaks at the interface. Previous observations of segregation of cobalt and chromium at stacking faults and microtwins were observed within γ' precipitates by high resolution TEM [39]. Similarly, the formation of η phase during creep was detected in γ' particles but not the γ matrix [40].

4.3. Formation of deformation twins

A number of recrystallized grains were found which showed the initial stages of the formation of a deformation twin. These grains were formed in a 'necklace' structure by dynamic recrystallization and were much smaller than the deformed grains, many less than 3μm in diameter as sectioned. The dislocation density varies depending on when these grains formed during the continuous compression of the samples. The twin-forming partials were observed in recrystallized grains containing other dislocations, not part of the twinning process, and were all found close to a grain boundary.

Figure 12a is a good example where a fan of overlapping partials is emitted from a low angle grain boundary. The low angle grain boundary (LAGB) forms a small wedge which does not pass through the full thickness of the foil, instead there is a sharp fold within the foil where the dislocations in the LAGB cross-slip onto the twinning plane

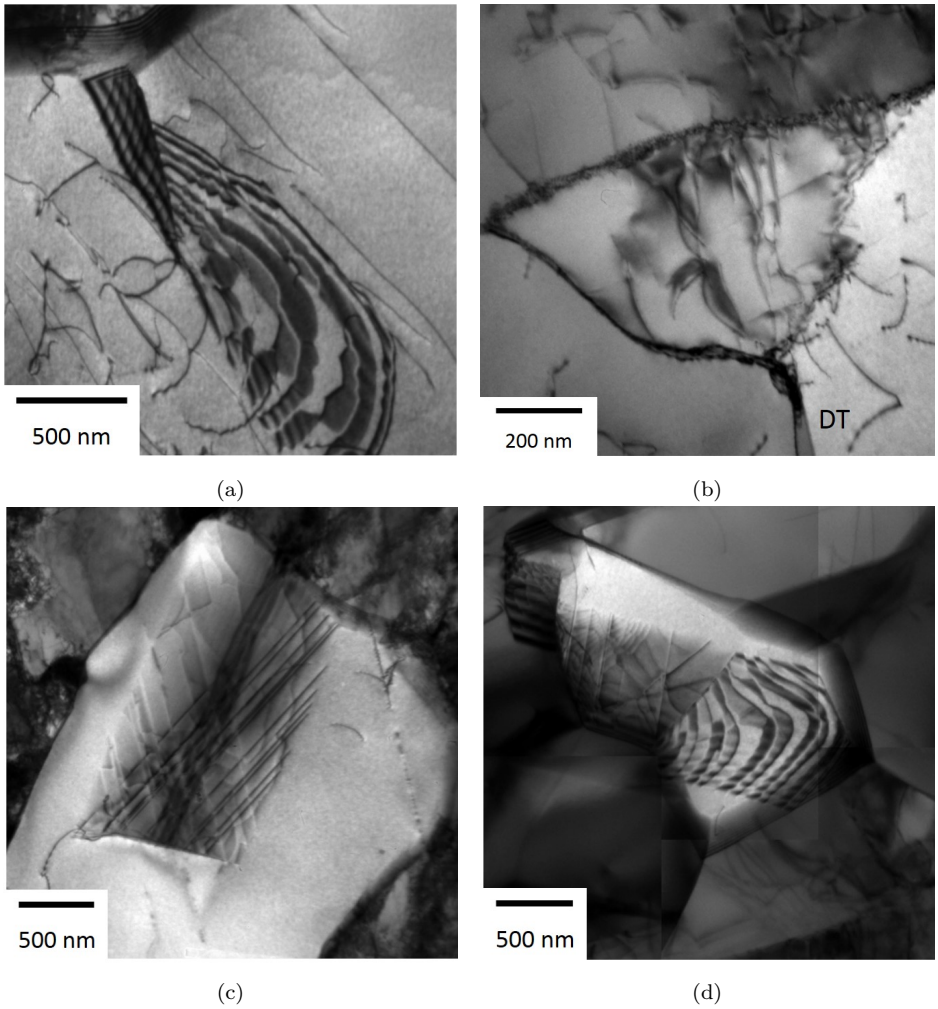

Figure 12. Nucleation sites for deformation twins in samples with the following testing parameters: (a) and (d) T=975°C, ϵ=1.2, $\dot{\epsilon}$=1 s^{-1} (b) T=1025°C, ϵ=1.2, $\dot{\epsilon}$=0.01 s^{-1} (c) T=950°C, ϵ=1.2, $\dot{\epsilon}$=1 s^{-1}

and the leading partials bow out to form the twin on the (111) plane. There is almost a one-to-one correspondence between the dislocations in the LAGB and the twinning dislocations, and the Burgers vectors are compatible.

It is notable that the dislocations only show the propensity to dissociate on the one plane not the plane of the LAGB. This could be due to the forces acting on the individual partials to constrict or expand the stacking fault, these forces would depend on the dissociation plane [27]. As with all the other early twinning events observed, it is close to a grain boundary.

A further example where a more irregular LAGB can serve as a twin nucleation site is shown in Figure 12b. This shows an edge-on deformation twin (marked with DT) emerging from the LAGB at the lower right side of the image. Grain boundaries can serve as nucleation sites for partial dislocations, especially important for nanocrystalline materials which are too small to provide a suitable length for a dislocation pile-up [14,41]. In the cases presented low angle grain boundaries emit twinning partials leaving trailing partials as part of the boundary, necessary to accommodate the misorientation of the emerging micro-twin.

Figure 12c presents overlapping twinning dislocations in the plane of the foil. The

alternating contrast of the twinning partials are marked by the red arrow. White arrows indicate straight dislocations on two different planes. The straight lines could be sessile dislocations. In a similar pattern these dislocations were determined to be Frank partials by Idrissi et al. [30]. Unfortunately, it was not possible to fully characterize them in the present image.

Figure 12d shows features discussed in a and c. The gray area on the left side of the white grain includes a number of faint and straight dislocations. This area is bordered with another straight line which is slightly tilted to the right. From this feature, fan-shaped stacking faults are emerging. Again, a low angle grain boundary is present in the vicinity of the twinning partials. However, the dislocations building the LAGB had no interaction with the partials of the stacking faults.

A wide range of nucleation mechanisms for deformation twins have been developed which require cross-slip events, pile-ups or dislocation reactions on co-planar planes [14]. The pole mechanism proposed by Venables [42] considers the formation of jogs as initiating configuration for twinning. A long jog in a dislocation splits into a sessile Frank partial of type $a/3\langle 111\rangle$ and a glissile Shockley partial $a/6\langle 112\rangle$. The Shockley partial can glide and bow around the jog leaving a stacking fault. The rotation around the poles creates stacking faults on adjacent planes with partials of the same Burgers vector forming the twin. Although this theory offers a solution for the formation of the necessary partials on adjacent planes, sufficiently large and mobile jogs are a prerequisite. Venables' pole mechanism still lacks experimental evidence [1]. Nucleation models based on twin formation on the primary slip plane rely on the formation of the correct partials on neighboring planes. Mahajan and Chin [3] presented a mechanism where co-planar dislocations dissociate into Shockley partials a process which is repeated on consecutive planes. It remains unclear though, what pins the trailing partial and how likely it is to form the ideal partial configuration on adjacent planes for twin formation. Another model proposing twin formation on the same plane as dislocation slip happens is from S. Miura, J. Takamura and N. Narita [43]. A key feature is the presence of a Lomer-Cottrell lock [44]. A Lomer-Cottrell lock is formed when two leading partials on conjugate planes encounter each other on an intersection of the slip planes forming a sessile Frank partial. In the Miura-Takamura-Narita model dislocations pile up ahead of the lock. When the leading dislocation encounters the lock it reacts with the sessile $a/3\langle 110\rangle$ to form two partials which double-cross-slip on adjacent planes and leaves behind a Frank partial. This model lacks an explanation for the second cross-slip event and subsequent growth cannot be explained either. The nucleation theories by J. Cohen and J. Weertman [45] and T. Mori and H. Fujita [46] consider twinning on conjugate planes. The models differ in the dissociation reactions at the cross-slip events. The Cohen-Weertman model is similar to Miura-Takamura-Narita proposing interaction of a dislocation with a Lomer-Cottrell lock and the formation of a Frank partial but only producing a single twinning partial, and this on a conjugate plane. In this theory, the existence of the lock-dislocation is ignored and the locked only serves its purpose as an obstacle in the microstructure. Mori and Fujita developed a model for the cross-slip of partial dislocations. Therefore, the partial splits at a dislocation bundle or multipole in a sessile stair-rod dislocation $a/6\langle 110\rangle$ and a Shockley partial which forms a stacking fault on the conjugate plane.

As for the present samples, the nucleation of deformation twins in recrystallized grains did not require the formation of pile-ups. Hence, theories considering only dislocation glide such as the Mahajan-Chin [3] or Miura-Takamura-Narita [43] will not be considered any further. The Cohen-Weertman [45] and the Mori-Fujita model [46] both consider cross-slip mechanisms with different dissociation reactions. Considering

the fan-shaped structure in Figure 12a which has a low angle grain boundary to the right. The dislocations within this boundary were identified as matrix dislocations of the type a/2 $\langle 101 \rangle$. Hence, the cross-slip mechanism by Mori and Fujita is unlikely to be active. The dissociation mechanism proposed by Cohen et al. [45] would suggest leaving behind a sessile Frank partial for each twinning dislocation. These a/3$\langle 111 \rangle$ dislocations cannot be on top of each other on adjacent planes as the resulting Burgers vector is energetically unfavorable. The sharp interface in the grains with the fan-shaped stacking faults was lacking in any signs of trailing, sessile dislocations. A detailed analysis of Idrissi et al. [30] on mechanisms operating in TWIP steels confirmed two of these mechanisms being active in their samples. In the present analysis we are looking at twinning at much higher temperatures than these examples and this will make a difference as to what is possible or indeed likely.

A theory which could explain the observation of the fan-like arrays of partial dislocations would be the pole-mechanism proposed by Venables [42]. The original theory considers the formation of an extensive jog as the initiating configuration for twinning. Such a long jog was considered to be formed in copper under tensile by approximately 20 dislocations which cut a dislocation on the same plane. This formation will then be a viable source for twin nucleation.

The rotation around the poles creates stacking faults on adjacent planes with partials of the same Burgers vector forming the twin. However, in the present samples it is unlikely that a dislocation was to form a jog of adequate length given the lack of deformation in the grains containing the twin nuclei.

An alternative single pole-type mechanism is proposed as follows. If an isolated partial intersects with a screw dislocation it forms a step equivalent to a (111) plane. When bowing around the dislocation, one part of the partial propagates at the initial plane while the other part of the partial glides on the adjacent plane. They both leave behind stacking faults on parallel planes if the trailing partial is left behind. It is shown in Figure 10 that in this alloy the partials of a glissile dislocation can under some conditions separate by more than 200μm. There is also evidence of trailing partials either stationary or counter-rotating as discussed in Venables but dismissed in favor of prismatic dislocation mechanisms. None of the available mechanisms fully explains all the features shown here.

Dislocation activity is a necessary pre-cursor to twinning but the generally low dislocation density observed where these early stage twins are forming suggests that the SFE energy is sufficiently low for partials to move creating twins at stresses similar to those for perfect dislocation movement, but where the orientation of the grain favors the separation of the partials.

Thus, we would argue that the requirement for twinning to be preceded by substantial work-hardening, put forward for TWIP steels [1], does not appear to be valid for this super-solvus superalloy as twin nuclei form in very lightly deformed grains. Indeed, twinning and dislocation activity appear to operate simultaneously where grains which are heavily twinned often also have high dislocation densities. Twinning and dislocation movement will of course experience different Schmid factors in each grain and twinning will also experience a tensile/compressive anisotropy, leading to the observed uneven distribution of both mechanisms in individual grains.

Twinning clearly makes an important contribution to the deformation of 718Plus, and although none of the existing theories satisfactorily fits all the observations, several common features have emerged. These are the prevalence of fan-like arrays of similar partials and the close association with low angle boundaries. It is also worth noting that the alloy shows an exceptionally low SFE and is being deformed in compression

at high temperatures

4.4. Summary

High temperature compression tests were carried out on a Ni-base superalloy. Deformation twins were found within the samples regardless of the high testing temperature and low strain rates. TEM techniques were used to analyze the conditions under which deformation twinning occurred. In addition, the initiation and growth of twinning partials is discussed. The following conclusions can be drawn from the present study.

- Deformation twinning was observed in 718Plus during high temperature compression tests at all strain rates (0.01-1 s^{-1}) and strains (0.4-1.2) and in the temperature range from 850 to 1025°C being above and below the γ' solvus temperature
- Twinning on multiple slip systems was active in samples containing a γ-γ' microstructure. This could be reasoned by the stress concentration of the γ' particles.
- Deformation twinning in 718Plus at elevated temperatures is believed to be due to a decrease in stacking fault energy with temperature.
- The stacking fault energy of 718Plus at 975°C was measured to be between 12 and 17 mJ m^{-2}
- Twinning partials were observed to be emitted from low-angle grain boundaries. Another possible nucleation site was determined to be a Frank-Read source, where the shear stresses favor separation of partials. The formation of deformation twins did not require a significant degree of work hardening.

4.5. Acknowledgements

The authors would like to acknowledge the support of Rolls-Royce Deutschland and Otto Fuchs KG for providing the material and also Rolls-Royce plc. and the EPSRC (Engineering and Physical Science Research Council) Strategic Partnership under EP/H022309/1 and EP/H500375/1.

References

[1] De Cooman BC, Estrin Y, Kim SK. Twinning-induced plasticity (twip) steels. Acta Materialia. 2018;142:283 – 362.
[2] Nordström J, Siriki R, Moverare J, et al. Deformation Twinning Behavior in High Ni-Austenitic Materials. Materials Science Forum. 2018;941:1591–1596.
[3] Mahajan S, Chin GY. Formation of deformatin twins in f.c.c. crystals. Acta Metallurgica. 1973;21:1353–1363.
[4] Haase C, Barrales-Mora LA. Influence of deformation and annealing twinning on the microstructure and texture evolution of face-centered cubic high-entropy alloys. Acta Materialia. 2018;150:88–103.
[5] Zhang D, Jiang L, Zheng B, et al. Deformation Twinning (Update). Elsevier Ltd.; 2016. December.
[6] Smith TM, Unocic RR, Deutchman H, et al. Creep deformation mechanism mapping in nickel base disk superalloys. Materials at High Temperatures. 2016;33(4-5):372–383.
[7] Moverare JJ, Johansson S, Reed RC. Deformation and damage mechanisms during ther-

malmechanical fatigue of a single-crystal superalloy. Acta Materialia. 2009;57(7):2266 – 2276.
[8] Hong H, Kang J, Choi B, et al. A comparative study on thermomechanical and low cycle fatigue failures of a single crystal nickel-based superalloy. International Journal of Fatigue. 2011;33(12):1592 – 1599.
[9] Pu E, Zheng W, Song Z, et al. Hot deformation characterization of nickel-based superalloy UNS10276 through processing map and microstructural studies. Journal of Alloys and Compounds. 2017;694:617–631.
[10] Jiang H, Dong J, Zhang M, et al. A Study on the Effect of Strain Rate on the Dynamic Recrystallization Mechanism of Alloy 617B. Metallurgical and Materials Transactions A: Physical Metallurgy and Materials Science. 2016;47(10).
[11] Eskandari M, Zarei-Hanzaki A, Szpunar J, et al. Microstructure evolution and mechanical behavior of a new microalloyed high mn austenitic steel during compressive deformation. Materials Science and Engineering: A. 2014;615:424 – 435.
[12] Edwards TEJ, Di Gioacchino F, Mohanty G, et al. Longitudinal twinning in a TiAl alloy at high temperature by in situ microcompression. Acta Materialia. 2018;148:202–215.
[13] Mahajan S. Formation of Deformation Twins in Metallic Crystals. Acta Metallurgica. 2005;49:2005.
[14] Mahajan S. Critique of mechanisms of formation of deformation, annealing and growth twins: Face-centered cubic metals and alloys. Scripta Materialia. 2013;68(2):95–99.
[15] Beyerlein IJ, Zhang X, Misra A. Growth Twins and Deformation Twins in Metals. Annual Review of Materials Research. 2014;44(1):329–363.
[16] Löhnert K. Einfluss der thermomechanischen Vorbehandlung auf die Eigenschaften der Nickelbasissuperlegierung A718Plus [dissertation]. Universität Erlangen-Nürnberg; 2011. Available from: http://www.hut-verlag.de/9783843901123.html.
[17] Cao WD, Kennedy RL. Recommendations for Heat Treating Allvac® 718Plus® Alloy Parts. 2006;.
[18] Casanova A, Hardy M, Rae CMF. Morphology and Kinetics of Grain Boundary Precipitation in Alloy ATI 718Plus®. 8th International Symposium on Superalloy 718 and Derivatives. 2014;:573–586.
[19] Kienl C, Casanova A, Messé OM, et al. Characterization of the initial stages of dynamic recrystallization in ati 718plus®. Proceedings of the 9th International Symposium on Superalloy 718 and Derivatives: Energy, Aerospace, and Industrial Applications. 2018; :405–420.
[20] Kennedy RL, Cao W, Bayha TD, et al. Developments in Wrought Nb Containing Superalloys (718 + 100F). Superalloys 2003. 2003;.
[21] Srinivasan D, Lawless LU, Ott EA. Experimental determination of TTT diagram for ally 718PLUS®. Superalloys 2012. 2012;3:759–768.
[22] Huang K, Logé RE. A review of dynamic recrystallization phenomena in metallic materials. Materials and Design. 2016;111.
[23] Pradhan SK, Mandal S, Athreya CN, et al. Influence of processing parameters on dynamic recrystallization and the associated annealing twin boundary evolution in a nickel base superalloy. Materials Science and Engineering A. 2017;700.
[24] Diologent F, Caron P. On the creep behavior at 1033k of new generation single-crystal superalloys. Materials Science and Engineering: A. 2004;385(1):245 – 257.
[25] Ma S, Carroll L, Pollock T. Development of phase stacking faults during high temperature creep of ru-containing single crystal superalloys. Acta Materialia. 2007;55(17):5802 – 5812.
[26] Yuan Y, Gu Y, Cui C, et al. Creep mechanisms of u720li disc superalloy at intermediate temperature. Materials Science and Engineering: A. 2011;528(15):5106 – 5111.
[27] Hull D, Bacon DJ. Introduction to dislocations. 5th ed. Elsevier Ltd.; 2011.
[28] ATI Allvac. 718Plus Data Sourcebook. ATI Special Metals LTd.; 2008.
[29] Messé O, Barnard J, Pickering E, et al. On the precipitation of delta phase in ALLVAC® 718Plus. Philosophical Magazine. 2014;94(10):1132–1152.
[30] Idrissi H, Renard K, Ryelandt L, et al. On the mechanism of twin formation in femnc

twip steels. Acta Materialia. 2010;58(7):2464 – 2476.
[31] León-Cázares FD, Kienl C, Rae CMF. Three dimensional reconstruction of planar deformation features from single electron micrographs. Metallurgical and Materials Transactions A. 2019;.
[32] Reed RC. The superalloys: Fundamentals and applications. Cambridge University Press; 2006.
[33] Kovarik L, Unocic R, Li J, et al. Microtwinning and other shearing mechanisms at intermediate temperatures in ni-based superalloys. Progress in Materials Science. 2009; 54(6):839 – 873.
[34] Kolbe M. The high temperature decrease of the critical resolved shear stress in nickel-base superalloys. Materials Science and Engineering: A. 2001;319-321:383 – 387.
[35] Zhang X, Grabowski B, Körmann F, et al. Temperature dependence of the stacking-fault Gibbs energy for Al , Cu , and Ni. Phys Rev B. 2018;224106.
[36] Shang SL, Kim DE, Zacherl CL, et al. Effects of alloying elements and temperature on the elastic properties of dilute Ni-base superalloys from first-principles calculations. Journal of Applied Physics. 2012;112(5).
[37] Rémy L, Pineau A, Thomas B. Temperature dependence of stacking fault energy in close-packed metals and alloys. Materials Science and Engineering. 1978;36(1):47 – 63.
[38] Mahajan S, Pande CS, Imam MA, et al. Formation of annealing twins in f.c.c. crystals. Acta Metallurgica. 1997;45(6):2633–2638.
[39] Smith TM, Esser BD, Good B, et al. Segregation and Phase Transformations Along Superlattice Intrinsic Stacking Faults in Ni-Based Superalloys. Metallurgical and Materials Transactions A. 2018;(June).
[40] Smith TM, Esser BD, Antolin N, et al. Segregation and Î· phase formation along stacking faults during creep at intermediate temperatures in a Ni-based superalloy. Acta Materialia. 2015;100:19–31.
[41] Zhu YT. Deformation Twinning in Nanocrystalline Metals. Journal of Materials Engineering and Performance. 2005;14(August):467–472.
[42] Venables JA. Deformation twinning in face-centred cubic metals. The Philosophical Magazine: A Journal of Theoretical Experimental and Applied Physics. 1961;6(63):379–396.
[43] Miura S, Takamura J, Narita N. The high temperature decrease of the critical resolved shear stress in nickel-base superalloys. Trans JIM. 1968;9(Suppl.):555.
[44] Cottrell A. Lx. the formation of immobile dislocations during slip. The London, Edinburgh, and Dublin Philosophical Magazine and Journal of Science. 1952;43(341):645–647. Available from: https://www.tandfonline.com/doi/pdf/10.1080/14786440608520220.
[45] Cohen J, Weertman J. A dislocation model for twinning in f.c.c. metals. Acta Metallurgica. 1963;11:996.
[46] Mori T, Fujita H. Dislocation reactions during deformation twinning in Cu-11at.% Al single crystals. Acta Metallurgica. 1980;28(6):771–776.